DBD Reactor Design and Optimization in Continuous AP-PECVD of HMDSO/N_2/N_2O Mixture

Petr Hotmar*, Hubert Caquineau†, Raphaël Cozzolino, Nicolas Gherardi‡
LAPLACE, Université Paul Sabatier

Abstract

Dielectric Barrier Discharge (DBD) assisted deposition of thin films is increasingly studied as a promising alternative to other non-thermal processes such as low-pressure PECVD or wet-coating. In this paper we demonstrate how optimizing gas injection in the DBD results in an improvement in the reactor performance. We propose to confine the precursor gas close to the deposition substrate by an additional gas flow. The performance of this design is studied though simulation of mass transport. To optimize the deposited thickness, gas cost and reactor clogging, we assess the influence of the confinement, total gas flow rate and DBD length. The confinement is found to reduce reactor clogging, even for long DBD, and increase the deposited thickness. This increase in thickness requires a proportionate increase in the gas flow rate, making the gas-cost the main limitation of the proposed design. We show, however, that by fine-tuning the operating conditions a beneficial compromise can be obtained between the three optimization objectives.

Keywords: *AP-PECVD, DBD, deposition rate, optimization*

1 Introduction

Plasma enhanced chemical vapor deposition has been widely used since the late 70's, with the development driven primarily by applications in the microeletronics industry. Since the late 90's there has been a growing interest in atmospheric pressure (AP) deposition under low-temperature discharge, especially in industrial areas where film quality requirements are not as stringent as in microelectronics. Working at AP offers several advantages: inexpensive

*email: hotmar@laplace.univ-tlse.fr
†email: caquineau@laplace.univ-tlse.fr
‡email: nicolas.gherardi@laplace.univ-tlse.fr

equipment, no pumps, lower energy foot-print and easier in-line integration in continuous production lines. Several operating methods have been described in the literature [1–4], from DC to microwave, direct or remote plasma, from corona to glow discharges. We focus our study on deposition assisted by direct homogeneous dielectric barrier discharge (DBD) in the Townsend regime [5]. Far from thermal equilibrium, the main advantage of such discharge is minimal heating of the process gas.

In previous work [6] we showed that slow diffusion is a major obstacle to the substrate-directed transport of active species generated in gas phase by the discharge. Thus, one way to increase the process efficiency is to modify the reactor design. While research on gas injection and flow configuration exists for plasma jets with substrate located in the post-discharge zone [1, 7–9], none is available for DBDs. In [10] we proposed to confine the precursor flow by an additional plasma gas stream so that the active species are created near the substrate, thus shortening their path to the deposition zone. In this paper we extend the analysis by providing a computational optimization study of an AP-DBD silica deposition process from the hexamethyldisiloxane (HMDSO) precursor in nitrogen, with nitrous oxide as the oxidant species. Three optimization objectives have been chosen based on industrial considerations. The first one, subject to maximization, is the deposited thickness. The confinement has an associated penalty: while it has a positive impact on the reactor clogging, additional gas is consumed for a given thickness. Thus, we choose gas cost per unit of deposited thickness and reactor clogging as the remaining objectives, which are subject to minimization.

In Sec. 2 we describe the reactor design, the model and the chemical mechanism used in the simulations. In Sec. 3 we discuss the confinement effects under various conditions and present the three-objective optimization results.

2 Reactor design and deposition model

2.1 T-injection DBD

As the deposition rate is directly proportional to the wall-normal flux of the depositing species, the aim of this work was to enhance the relevant transport mechanisms and offer suggestions on performance-optimized reactor design. The precursor injection should be located close to the substrate to minimize stray deposition on the competing walls. Our goal was to hydrodynamically confine the precursor near the deposition area, thus increasing substrate-normal mass flux of reaction intermediates (radical species) due to their higher near-substrate concentration. Fig. 1 shows a 2-D cross-section of the reactor with the proposed T-injection.

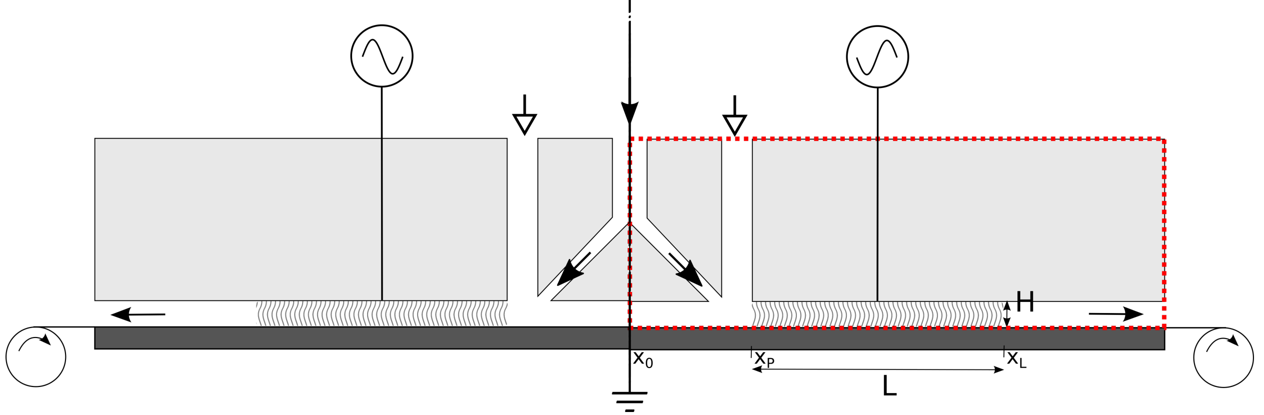

Fig. 1: 2-D cross-section of the plasma reactor with T-injection of the confining stream. The computational domain is denoted by a dotted box, vertical symmetry axis on the left. The wavy lines indicate DBD zones.

While the precursor mixture (HMDSO in N_2/N_2O) is introduced through angled inlet ports, the rest of the carrier gas (N_2/N_2O) enters through the slits oriented perpendicular to the moving substrate. Such an injection head provides a confining stream which blankets the precursor stream in the deposition region. The mixture then continues into DBD for deposition. While the gap height of the DBD is fixed at $H = 1$ mm and its width at $W = 3$ cm, its length, L, is subject to optimization. An added benefit of this design is an increase in the residence time of the precursor molecules and radicals as they are being convected on the streamlines in close proximity to the substrate and thus travel at lower velocity. Due to the inherent axial symmetry of the reactor and gas flow, the computational domain is restricted as shown in Fig. 1.

An alternative confinement with a showerhead upper-electrode was also studied and its performance found inferior to the T-injection design, except for short DBD. Indeed, the homogeneous distribution of the confinement flow through numerous showerhead jets yields low convection especially close to the entrance of the DBD. This, in turn, results in low HMDSO concentration close to the substrate, when compared to the case where the entire confinement stream is injected through a single inlet.

The nominal operating conditions are based on [6] and include peak voltage $V_{RF} = 6$ kV and frequency $f = 5$ kHz, yielding $P = 1$ W/cm^2 of the deposited power density. A straightforward way to achieve high deposition rate irrespective of the confinement studied in this work would be to maximize the amount of entering precursor by increasing gas flow rate and precursor concentration. Nevertheless, the gas flow rate Q is limited to a realistic maximum of 16 slm and precursor concentration in the precursor inlet line, x_{A0}, is kept at 40 ppm, i.e. slightly lower than the upper limit of 50 ppm for homogeneous

discharge stability [5]. Furthermore, the changes in power and HMDSO concentration have been studied extensively [6] within the standard experimental ranges and found to have no influence on the qualitative trends investigated in this work.

2.2 Model description

Modeling a plasma-enhanced chemical vapor deposition process at atmospheric pressure (AP-PECVD) is a non-trivial task largely due to a strong coupling of several physics processes, including plasma discharge and deposition dynamics. Multiple length and time scales lead to stiff, nonlinear systems with severe time-step constraints. Numerous model simplifications and suitable numerical techniques are thus required to make the problem tractable. Substantially different time scales [11] allow us to decouple the discharge dynamics from the mass and momentum transport of neutral species.

In this work the results from a plasma discharge model are used to provide source terms for the simulation of the reactive transport of chemical species. Time-dependent plasma fluid equations are solved in 1D, pure nitrogen (due to negligible concentration of the other species [12]) and for the electric parameters specified above, until periodic steady state is reached. The reactive flow of multi-component gas is modeled under steady-state conditions. A 3D to 2D reduction in dimensionality is exploited for computational efficiency due to a large aspect ratio of the reactor ($W \gg H$). We assume pseudo-steady, incompressible (Mach number $Ma = U/c \sim 10^{-2} \ll 1$, with speed of sound c), laminar flow of Newtonian fluid, governed by the Navier-Stokes and mass conservation equations,

$$\rho\left(\boldsymbol{u}\cdot\nabla\right)\boldsymbol{u} = \nabla\cdot\left[-p\boldsymbol{I} + \mu\left(\nabla\boldsymbol{u} + (\nabla\boldsymbol{u})^T\right)\right] \tag{1}$$

$$\rho\nabla\cdot\boldsymbol{u} = 0, \tag{2}$$

with density ρ, fluid velocity $\boldsymbol{u}$, pressure p and dynamic viscosity μ. With Reynolds number $Re = UH/\nu \sim 10^2$, where ν is the kinematic viscosity, convective momentum transfer dominates over the diffusive momentum transfer, yielding approximately inviscid flow. The conservation of diluted chemical species, combined with the Fick's law, yields

$$\nabla\cdot(-D_i\nabla c_i) + \boldsymbol{u}\cdot\nabla c_i = R_i, \tag{3}$$

with diffusion coefficient D_i and reaction rate R_i.

The boundary conditions for the fluid flow are no-slip at the walls, normal inflow velocity at the inlets and atmospheric pressure with vanishing viscous stress at the outlet. For the mass transport, the walls experience fluxes given by the surface chemistry, inlets are

assigned prescribed concentrations and outlets exhibit vanishing diffusive flux (standard open boundary condition). Zero-flux boundary conditions are assigned at the symmetry axis.

The system is solved with finite element method (Comsol) and includes procedures for stabilization of pressure oscillations (Galerkin least squares) and smoothing of concentration discontinuities.

The chemical mechanism considered for this model has been described in [6] and is outlined below. Since 1D discharge simulation [12] predicts low density and mean energy (≈ 4 eV) of electrons, we consider the $\mathrm{N_2}\,(A^3\Sigma_u^+)$ species as the primary agent responsible for HMDSO dissociation. The products include a radical species with a preserved Si-O-Si structure of HMDSO, Si_v, and a generic by-product Y_1:

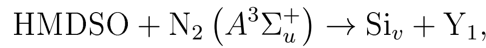

$$\mathrm{HMDSO} + \mathrm{N_2}\left(A^3\Sigma_u^+\right) \rightarrow \mathrm{Si}_v + \mathrm{Y}_1,$$

with the reaction rate $\mathrm{k}_g = 4 \times 10^{-11}$ $\mathrm{cm^{-3}s^{-1}}$ [6]. While the concentration of $\mathrm{N_2}\,(A^3\Sigma_u^+)$ is obtained from the plasma model, for the Si_v species reacting at the surface we assume complete oxidation to the depositing dimer of $\mathrm{SiO_2}$:

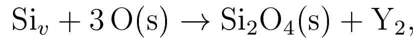

$$\mathrm{Si}_v + 3\,\mathrm{O(s)} \rightarrow \mathrm{Si_2O_4(s)} + \mathrm{Y}_2,$$

with the reaction rate $R_{surf} = 1/4\,\gamma\, c_{Si_v} v_{th}$, where $\gamma = 1$ is the sticking coefficient and v_{th} the thermal speed of Si_v.

The aim of such simplified reaction chemistry is to qualitatively capture the behavior of the deposition process without including low-impact species. In addition, current research provides little information on HMDSO decomposition and subsequent reactions. Finally, this mechanism allows us to reproduce the deposition rate profiles under operating conditions compatible with [6]. The validity of this mechanism relies on the preservation of the Si-O-Si structure in Si_v and its oxidation at the surface. Since the publication of [6], the decomposition of HMDSO has been addressed in [13–17]. Radicals with a single silicon atom resulting from the breakage of the Si-O bond have been hypothesized as film precursors in [15–17]. In those works, however, the operating conditions differ from ours, as does the carrier gas (He [15, 16] and/or Ar [17]). While the initiation reaction of HMDSO dissociation remains unclear (direct electron impact versus reaction with metastable species) [16], operating in those rare gases leads to electron and metastable species with higher energy than in nitrogen. The typical metastable energies of He and Ar metastables are, respectively, on the order of 20 eV and 10 eV, suggesting a sufficient part of the electron population should reach the ionisation energy (24.59 eV in He and 15.76 eV in Ar) to operate in the Townsend regime.

With bond energies of Si-C and Si-O at 4.53 eV and 8.31 eV, respectively [17], the discharge in He and Ar can possibly break either Si-O or Si-C bonds. The 6.3 eV energy of N_2 $(A^3\Sigma_u^+)$ metastables, the species we consider to be the cause of the dissociation, exceeds energy required to break Si-C bond, but not the Si-O bond. Supporting our hypothesis, Jauberteau and Jauberteau [17] showed that the dissociation process becomes selective toward Si-C bond breaking when HMDSO interacts with photons in the energy range from 7.3 eV to 10 eV; this is preferential to the reaction with $Ar(^3P_2)$ metastables (11.55 eV), which leads to additional Si-O breaking. Regarding our hypothesis on surface oxidation, Reuter et al. [18, 19] and Fanelli et al. [13, 14] emphasized the key role of surface oxidation in lowering carbon content in deposited layers. In our experiments the FTIR signature of the deposited films was nearly identical to silica.

The main objective of this work is to show how confinement can increase reactor performance in terms of the deposited thickness, gas cost and/or clogging of the reactor. Because the deposition occurs over a rolling web, a convenient indicator of the deposition efficiency is the total thickness deposited, t_d, upon web exit from the DBD:

$$t_d = \frac{1}{v_w} \int_0^L v_d(x) dx, \tag{4}$$

where v_d is the deposition rate and x is the distance from the DBD entrance. The web speed v_w acts as a scaling factor and the results presented here use the value of $v_w = 1$ m/min. The gas cost, c_g, is expressed in units of slm per deposited nanometer:

$$c_g = \frac{Q}{t_d}, \tag{5}$$

where Q is the total gas flow rate in slm. The maximum deposition rate over the electrode not coated by the web (the upper electrode in Fig. 1) represents the clogging of the reactor, c_r.

The total gas flow is split between two inlets. We define a confinement rate, $\mathcal{C}$, as the fraction of the total gas flow Q that enters through the vertical inlet Q_v, $\mathcal{C} = Q_v/Q$. For $\mathcal{C} = 0$ the flow is unconfined and admitted through the precursor entrance. Unless stated otherwise, the parametric ranges used in this work are as follows: confinement ratio $\mathcal{C} \in \langle 0, 0.1, \dots 0.9 \rangle$, DBD length $L \in \langle 0.004, 0.006, \dots 0.03 \rangle$ m, and gas flow rate $Q \in \langle 2, 3, \dots 16 \rangle$ slm.

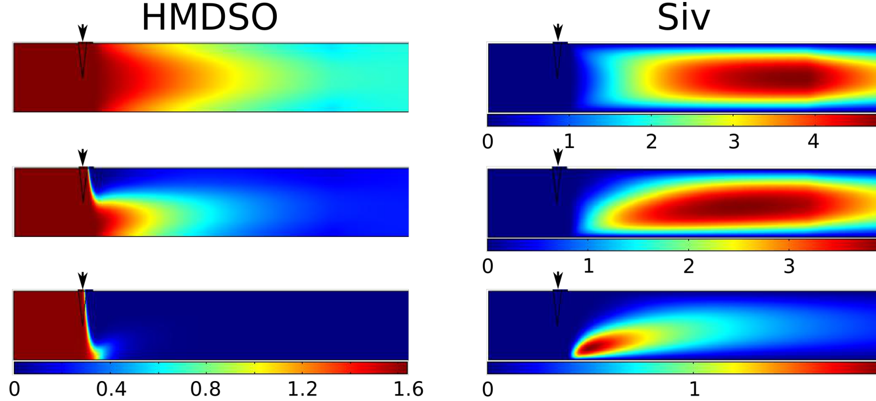

Fig. 2: Dependence of concentration of HMDSO (left column) and Si_v (right column) in the DBD region on the confinement ratio: $\mathcal{C} = 0$, 0.4 and 0.9 (from top to bottom). $Q = 4$ slm, $L = 3$ cm and $x_0 = 40$ ppm. The length-to-width ratio was scaled to show the entire DBD; arrow indicates the location of the precursor inlet. The scales for HMDSO contours are identical and given in 10^{-3} mol m^{-3}, the scales for Si_v contours are given in 10^{-4} mol m^{-3}.

3 Confinement effects

The influence of confinement on the concentration of precursor and radical species is shown in Fig. 2. As expected in laminar flow under confinement, near the DBD entrance the HMDSO stream is compressed close to the moving web. Due to low strain and vorticity normal to the interface, the mixing of the two co-flowing streams occurs primarily by diffusion, which hinders immediate deposition near the entrance. Thus, as $\mathcal{C}$ increases, we observe several related effects. First, Si_v reaches its maximum concentration progressively closer to the substrate. Second, the amount of HMDSO entering the reactor decreases (e.g. for $\mathcal{C} = 0.9$ it is 10 times smaller than without confinement), leading to a corresponding decrease in its maximum concentration and to earlier consumption. This, in turn, leads to a steeper drop of the deposition rate after it reaches its maximum, which grows and moves towards the entrance; this is shown in Fig. 3, which depicts deposition rate profiles for several $\mathcal{C}$ values.

Deposition on a rolling web is, however, best represented by measures based on the integral of the deposition rate profiles. In addition to the deposit thickness t_d defined previously in Eq. (4), we define a non-dimensional parameter,

$$\epsilon = \frac{t_d}{t_d^0}, \tag{6}$$

as a measure of the confinement efficiency, which relates the deposit thickness t_d to that obtained without the vertical confinement, t_d^0. For a consistent comparison of the deposit thickness with and without confinement for a specific value of $\mathcal{C}$, we retain the same molar flow rate of HMDSO in both cases, i.e. $x_{A0}(1 - \mathcal{C})Q$.

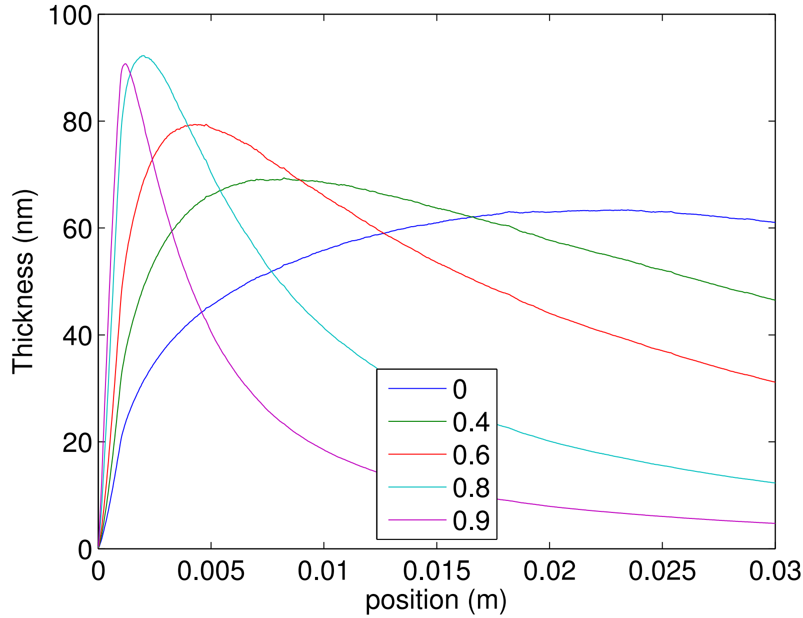

Fig. 3: Deposition rate profiles as functions of position in the DBD for different values of $\mathcal{C}$. Note the growth in the maximum given sufficient amount of HMDSO ($\mathcal{C} \leq 0.8$). $Q = 4$ slm, $L = 3$ cm.

Fig. 5 shows the deposit thickness t_d, gas cost c_g, reactor clogging c_r and confinement efficiency ϵ as functions of $\mathcal{C}$ for variable length L and flow rate Q. When discussing the influence of a single parameter in the remainder of this section, the other parameters are kept fixed unless stated otherwise.

The deposit thickness (Fig. 5a) increases with the reactor length L because identical deposition rate profiles are integrated over a progressively longer x-coordinate. The dependence on $\mathcal{C}$ shows a unimodal profile. The increasing part of the curve is a direct consequence of the confinement which forces the depositing species closer to the substrate, thereby increasing the species mass flux normal to the wall at which the surface deposition occurs. The curve starts decreasing when the preferential deposition on the substrate (mass gain due to limited stray deposition) can no longer compensate for the mass loss of the precursor due to dilution. To facilitate further analysis, we define the optimal confinement rate as

$$\mathcal{C}_{opt} = \arg\max_{\mathcal{C}} \, t_d. \tag{7}$$

The different thickness profiles in Fig. 3 illustrate the issues with operating in the region where $\mathcal{C} \geq \mathcal{C}_{opt}$: as confinement increases further, extending electrode length yields progressively smaller benefits in terms of deposit thickness (e.g. negligible gain in t_d for $\mathcal{C} = 0.9$ and $Q = 4$ slm) due to a progressively steeper drop in the deposition rate.

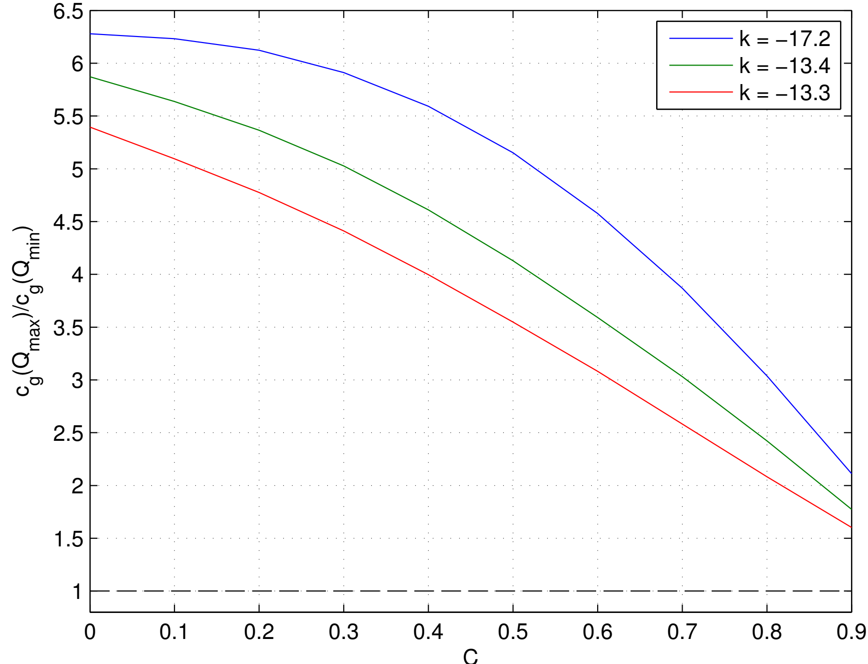

Fig. 4: Gas cost ratio $R = c_G(Q_{max})/c_G(Q_{min})$ for $L = 1$, 2 and 3 cm in blue, green and red, respectively. Curve derivatives k evaluated at $\mathcal{C}_{opt}$ for $t_D(L, Q_{max})$ confirm approach to a constant limiting value of $R = 1$.

As t_d improves with DBD length, so does the gas cost c_g. Fig. 5b shows a favorable decrease in c_g especially at high flow rates and low confinement due to the deposition rate profile being almost uniform across the reactor length (cf. Fig. 3 for $\mathcal{C} = 0$ or $\mathcal{C} = 0.4$). It is worth noting that as L increases, the c_g curves approach one another, indicating improved gas usage. Indeed, as shown in Fig. 4, with increasing electrode length the ratio R of gas costs for different flow rates approaches unity, first for high $\mathcal{C}$, and ultimately also for low $\mathcal{C}$. In the limit, we obtain $\lim_{L\to\infty} R = 1$, indicating maximum conversion (as dictated by the reaction chemistry) has been reached and all additional mass contained in the flow rate difference has been, upon reaction, deposited.

Of all the parameters of interest the reactor clogging, c_r (Fig. 5c), is the one most sensitive to the confinement, especially for small $\mathcal{C}$ and short DBD. A monotonously decreasing dependence of c_r on $\mathcal{C}$ confirms a key benefit of this reactor layout, namely that increasing the deposit thickness by optimizing $\mathcal{C}$ also reduces reactor clogging.

Fig. 5d shows that the confinement invariably leads to an improvement in the deposit thickness: $\epsilon \geq 1$, where the equality holds for $\mathcal{C} = 0$. The maximum efficiency, $\epsilon_{max} = 1.8$, is reached for high flow rates and short DBD. The locations of maxima in $t_d(\mathcal{C})$ and $\epsilon(\mathcal{C})$ (see Eq. 6), do not coincide because the maxima in t_d occur due to a different mechanism than those in t_d^0. While without confinement the lower flow rate increases residence time during

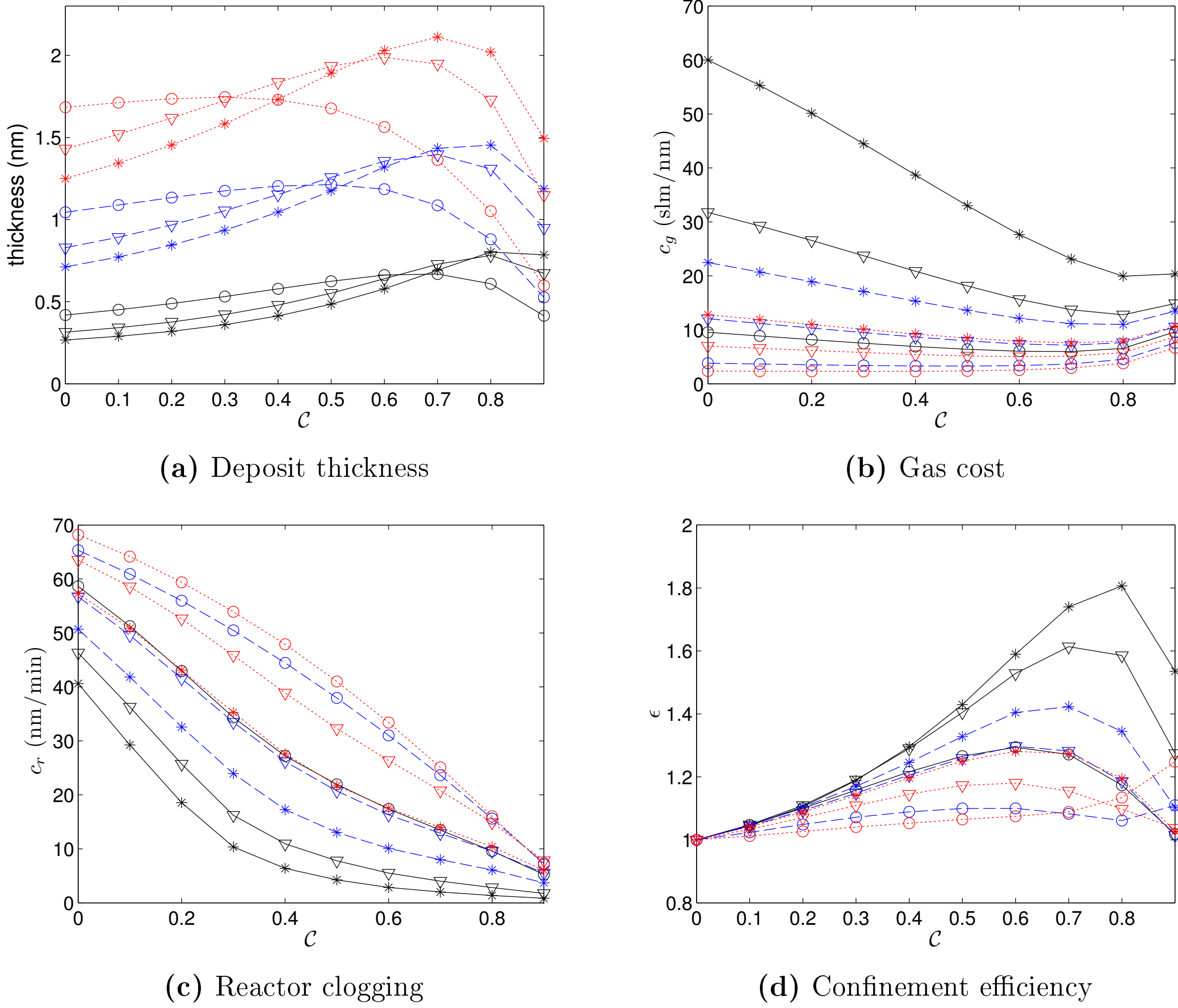

(a) Deposit thickness

(b) Gas cost

(c) Reactor clogging

(d) Confinement efficiency

Fig. 5: Deposit thickness t_d, gas cost c_g, reactor clogging c_r and confinement efficiency ϵ as functions of $\mathcal{C}$ for $L = 1, 2$ and 3 cm (resp. in solid black, dashed blue and dotted red) and $Q = 4, 10$ and 16 slm (resp. denoted with circles, triangles and stars).

which species can deposit, such a setup no longer enjoys confinement-provided increase in wall-directed mass flux. The confinement is thus beneficial primarily where residence time is short, either due to fast flow rates or short electrodes. The opposite scenario ($Q = 4$ slm and $L = 2$ or 3 cm) results in $\mathcal{C}_{opt}(t_d^0) < \mathcal{C}_{opt}(t_d)$ and $\arg\max \epsilon(\mathcal{C}) = \mathcal{C}_{max} = 0.9$, thus giving a confinement value prohibitively large from the gas cost perspective.

To gain more insight into how the maxima of quantities depicted in Fig. 5 vary with Q and L, we define

$$t_d^\star = t_d(\mathcal{C}_{opt}), \qquad c_r^\star = c_r(\mathcal{C}_{opt}), \qquad c_g^\star = c_g(\mathcal{C}_{opt}), \qquad F^\star = C_0 Q(1 - \mathcal{C}_{opt}), \tag{8}$$

where C_0 is the precursor concentration at the inlet.

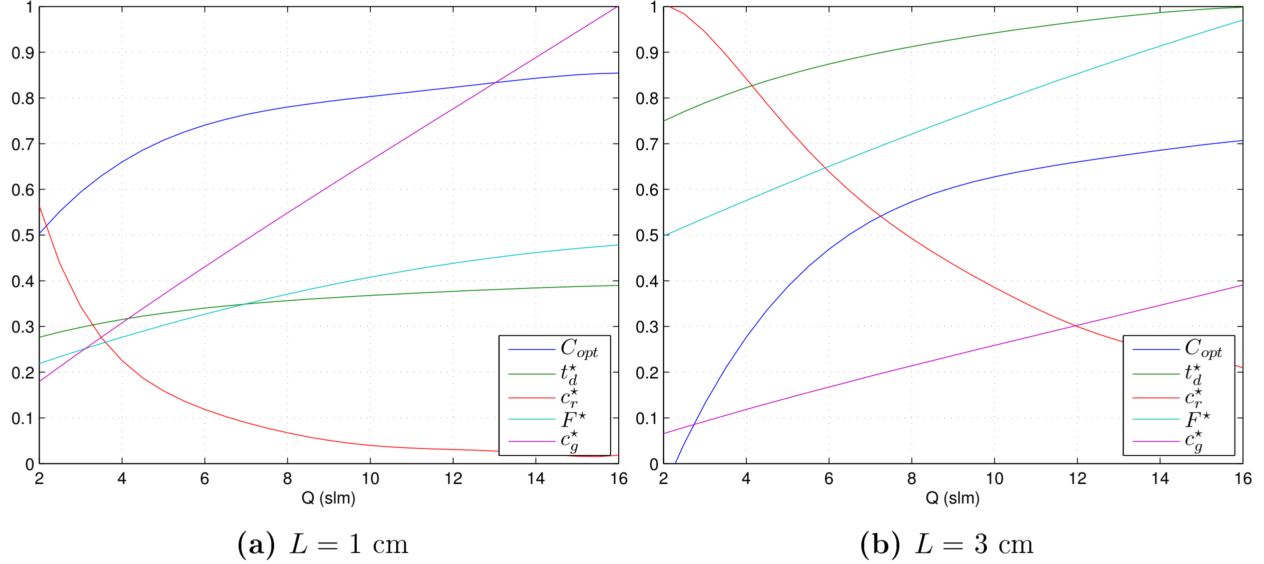

(a) $L = 1$ cm

(b) $L = 3$ cm

Fig. 6: Optimal confinement conditions to obtain maximum deposit thickness. The values of $t_d^\star$, $c_r^\star$, $c_g^\star$ and $F^\star$ are normalized by their maxima of 2.12 nm, 64.5 nm/min, 19.3 slm/nm and 7.85×10^{-6} mole/min, respectively.

Fig. 6 shows, for several reactor lengths, the Q-dependence of $\mathcal{C}_{opt}$ and of the values $t_d^\star, c_r^\star, c_g^\star$ and $F^\star$ normalized to $(0, 1)$ range. For a fixed length L, increasing Q from 2 to 16 slm increases $t_d^\star$ approx. by a factor of 1.4, which is related to the increase in $F^\star$. This suggests that when the proportionate gas cost increase is acceptable (e.g. for an expensive precursor), the confinement we propose is a viable option, especially at low flow rates, where the increase in t_d is more pronounced. Indeed, for the 3-cm DBD, the yield in deposited thickness per mole of entering precursor increases by a factor of 1.41 and 1.76 at 7 slm and 16 slm, respectively, compared to the yield at 2 slm. The associated reduction in reactor clogging is significant: under the optimal conditions discussed above, the confinement reliably protects the non-coated electrode from parasitic deposition, even in long DBD reactors. As expected, the gas cost is inversely proportional to the reactor clogging: as Q is increased to obtain higher deposition rate, c_g increases correspondingly. Longer DBDs then provide partial remedy, increasing the conversion and thus the efficiency of gas usage.

3.1 Optimization

To perform a more detailed multi-objective optimization of mutually-conflicting measures represented by the three criteria defined above, i.e. the deposit thickness, gas cost and reactor

clogging, we introduce a composite objective function $\beta(\mathcal{C}, Q)$ based on a linear scalarization,

$$\beta = \sum_{i=1}^{3} \boldsymbol{w_i f_i}, \tag{9}$$

where $\boldsymbol{f} = \{t_d^*, -c_g^*, -c_r^*\}$ are normalized objective functions and $\boldsymbol{w} = \{w_1, w_2, w_3\}$ are the respective weights that satisfy $\sum_i w_i = 1$. Defining a solution vector $\boldsymbol{x} = (\mathcal{C}, Q)$ for a given weight combination with the domain $\boldsymbol{X} = \boldsymbol{x} : \{0 \leq \mathcal{C} \leq 0.9, 2 \leq Q \leq 16 \text{ slm }\}$, the optimal solution is obtained as

$$\boldsymbol{x}_{opt} = \underset{\boldsymbol{x} \in \boldsymbol{X}}{\arg\max}\ \beta(\boldsymbol{x}). \tag{10}$$

The choice of scales used to normalize the objective functions is critical, and was based on the results shown in Fig. 5. For the deposit thickness, the scaling factor is 1 nm, the typical order of magnitude of t_d. As scales for c_g and c_r we chose 10 slm/nm and 10 nm/min, respectively.

Figs. 7-9 shows the optimum values for $\mathcal{C}$ and Q and the corresponding values for t_d, c_g, c_r and ϵ as functions of w_1, w_2 and w_3. These figures should be interpreted the same way as ternary diagrams: to determine e.g. w_1, draw a parallel to the triangle side opposite to the $w_1 = 1$ apex and locate its intersection with the w_1 axis.

The confinement is very efficient in limiting the reactor clogging, as evidenced by the large area of the low c_r region ($c_r < 20$) in Figs. 7-9e. This holds true even when optimizing the deposit thickness, which requires lower confinement: $\mathcal{C} = 0.8$ for $L = 1$ cm and $\mathcal{C} = 0.7$ for $L = 3$ cm; optimizing c_r gives $\mathcal{C} = 0.9$, irrespective of the remaining criteria.

In contrast, prioritizing the gas cost, which is primarily determined by the flow rate of plasma gas Q (Figs. 7-9b), imposes reduction in confinement, especially as $w_2 \to 1$. In particular, for $L = 1$ cm, the areas of constant Q^* closely mimic those of constant c_g, with the deviation from constant w_2 coordinate lines increasing as $w_2 \to 1$. As L increases the transition between low and high flow rate regions changes from gradual to almost step-wise, with only 2-slm and a 16-slm regions, the latter covering most of the triangle. In addition, while the low-c_g region (Fig. 9d) contracts, the high-t_d region (Fig. 9c, $t_d \geq 1.8$ nm) grows. For $w_1 = 1$ (where $t_d = t_{d,max} = 2.11$ nm and $c_r = 14$ nm) we obtain high confinement efficiency, $\epsilon = 1.3$. The main disadvantage of operating near this vertex is the gas cost, $c_g = 7.6$ slm/nm. For $Q = 2$ slm without confinement we obtain smaller deposit thickness $t_d = 1.6$ nm and strong clogging, at the benefit of gas cost savings, $c_g = 0.8$ slm/nm. The vicinity of the high-to-low flow rate transition is particularly interesting as it offers a good compromise among the three objectives. As an example, operating with $\boldsymbol{w} = (0.26, 0.64, 0.1)$ allows depositing 2 nm with a relatively low clogging of 19 nm/min and a reasonable gas cost

of 5.5 slm/nm, compared to 7.6 slm/min required to obtain the maximum deposit thickness of 2.1 nm.

To evaluate how the reactor length should be varied to maximize the composite objective, we introduce L as an additional optimization criterion, yielding $\beta(\mathcal{C}, Q, L)$; the optimal solutions are shown in Fig. 10. In general, the most efficient DBD design favors long reactors and high flow rates, confirming the conclusions given above for $L = 3$ cm. The exception is the case where reactor clogging is of interest. While gas cost favors reduction in the flow rate, limiting reactor clogging requires reduction of the DBD length. We confirm that c_r remains low except close the $w_2 = 1$ vertex; this is the result of high confinement, $\mathcal{C} \geq 0.7$, across most of the optimization triangle.

4 Conclusions

In this work we performed a computational study with the aim to optimize a design of gas injection in DBD used to deposit SiO_2-like layers on a moving web in N_2/N_2O/HMDSO. The proposed design relies on the confinement of the precursor flow by an additional stream of N_2/N_2O. We studied the effects of the confinement factor $\mathcal{C}$, total gas flow rate Q and DBD length L on the deposit thickness t_d, gas cost c_g, reactor clogging c_r confinement efficiency ϵ. We showed that the confinement provides an efficient method to increase the deposit thickness and also lower reactor clogging. The main cost associated with the proposed design is gas consumption, making this method especially economically viable especially where the precursor is expensive and its efficient use is thus desirable.

An additional, three-objective (t_d, c_g and c_r) optimization study was performed in the $\{\mathcal{C}$,$Q\}$ space. It confirms that high deposited thickness can be achieved simultaneously with low reactor clogging and requires high confinement, typically $\mathcal{C} \geq 0.7$. Reducing gas cost c_g is the main motivation to lower $\mathcal{C}$. Nevertheless, it is possible, by fine-tuning $\mathcal{C}$ and Q, to obtain good compromise between gas cost c_g and deposited thickness t_d (or reactor clogging c_r); the resulting confinement efficiency ϵ is then approx. 1.2. Efficiency as high as $\epsilon = 1.8$ can be achieved for short DBDs, at the expense of increased c_g. Increasing DBD length lowers ϵ because longer residence times allow for higher conversion even without confinement. A complementary study in the $\{\mathcal{C}, Q, L\}$ space provided suggestions on how to optimize DBD length. While t_d and c_g benefit from longer electrodes, c_r exhibits the opposite trend.

The reaction chemistry adopted, to which the results show great sensitivity, is supported by good agreement between simulation and experimental results, and provides a general insight in the consequences of using alternate gas injection configuration in a direct DBD deposition process. The proposed optimization procedure provides the practitioner with a

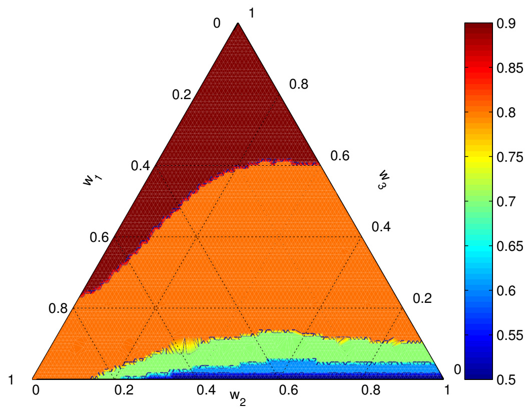

(a) optimum $\mathcal{C}$

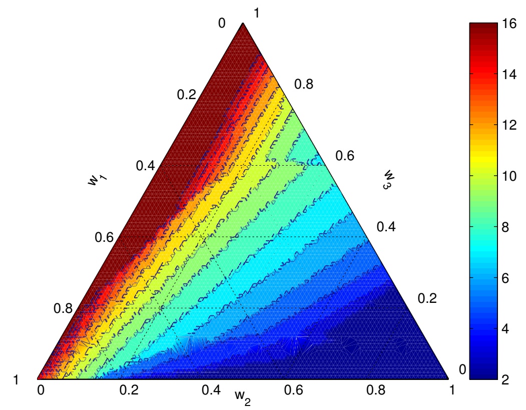

(b) optimum Q

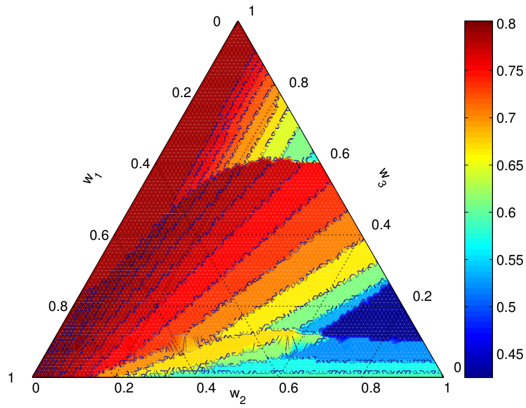

(c) t_d

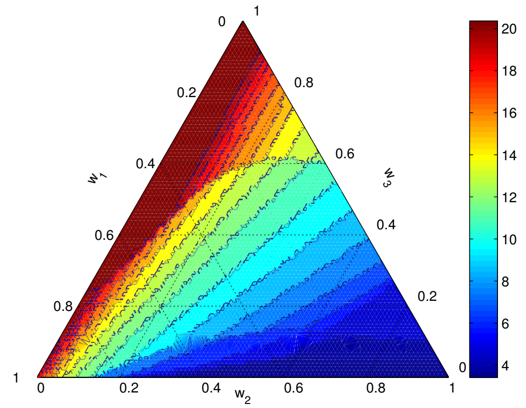

(d) c_g

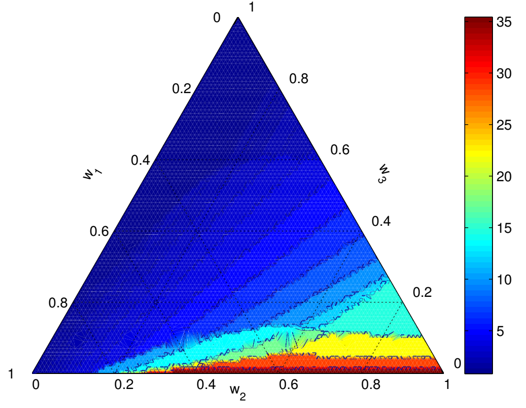

(e) c_r

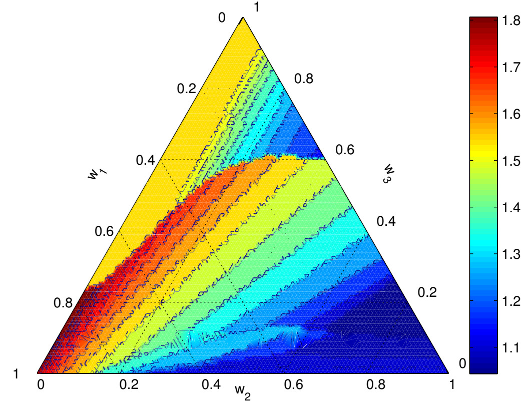

(f) ϵ

Fig. 7: Optimization results for $L = 1$ cm.

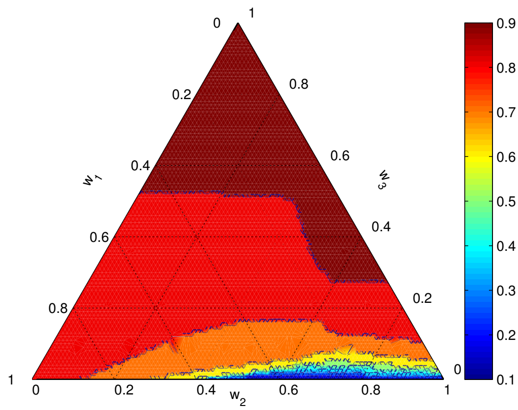

(a) optimum $\mathcal{C}$

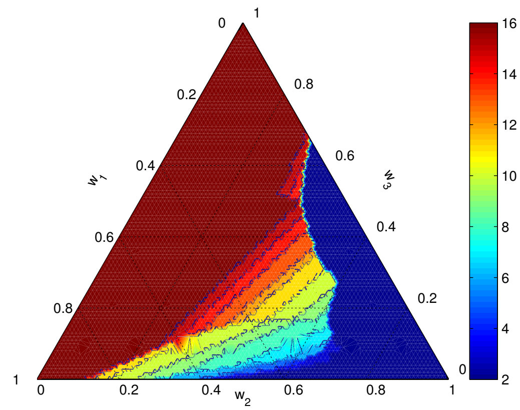

(b) optimum Q

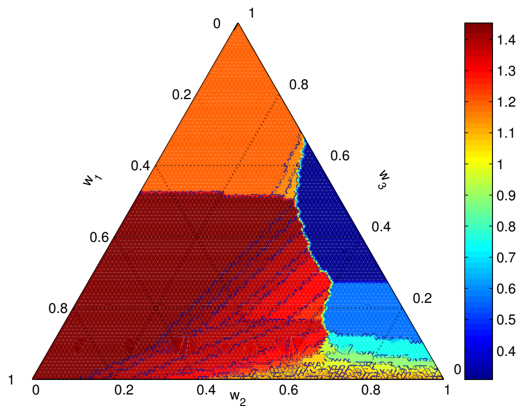

(c) t_d

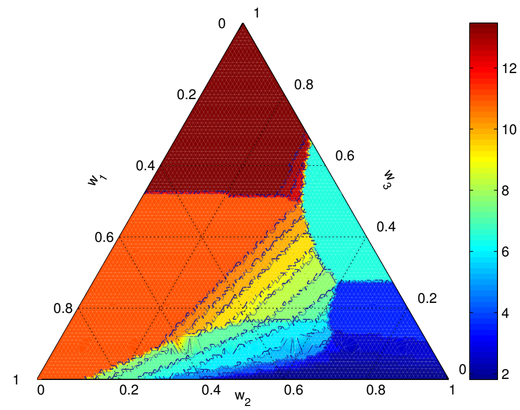

(d) c_g

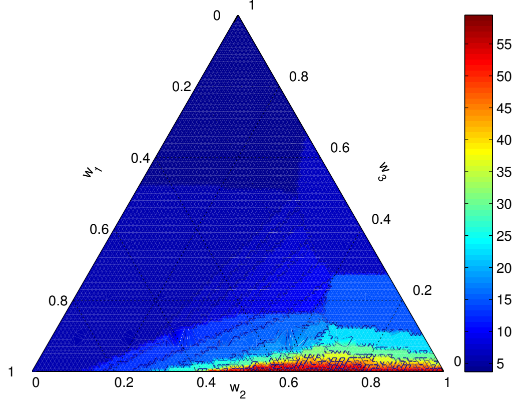

(e) c_r

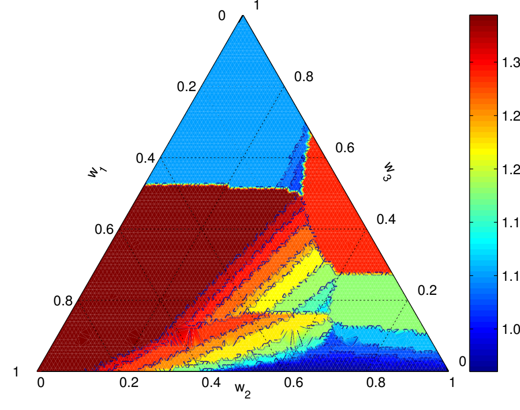

(f) ϵ

Fig. 8: Optimization results for $L = 2$ cm.

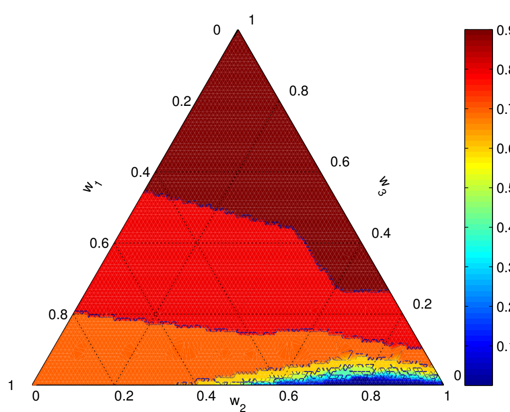

(a) optimum $\mathcal{C}$

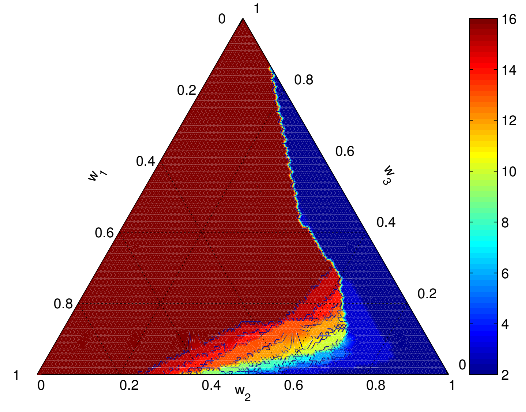

(b) optimum Q

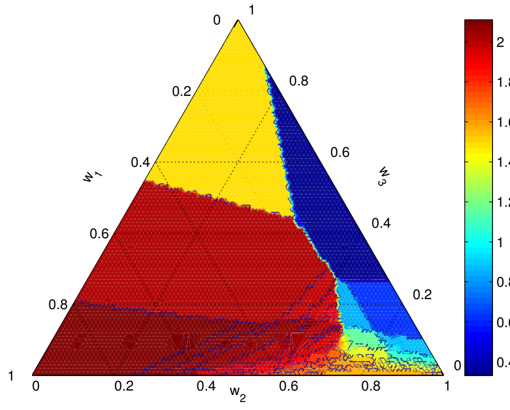

(c) t_d

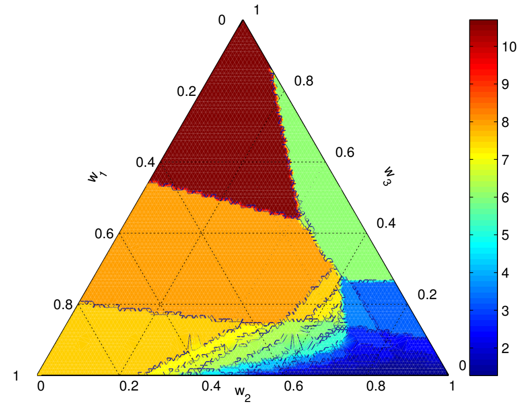

(d) c_g

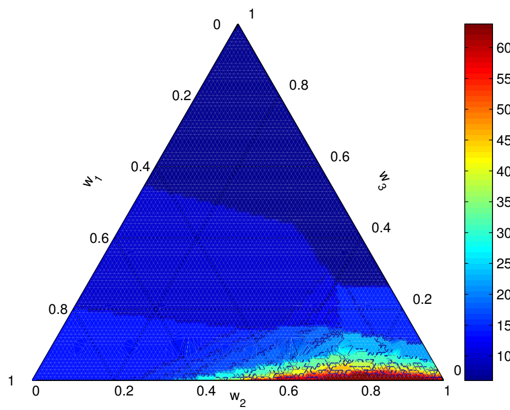

(e) c_r

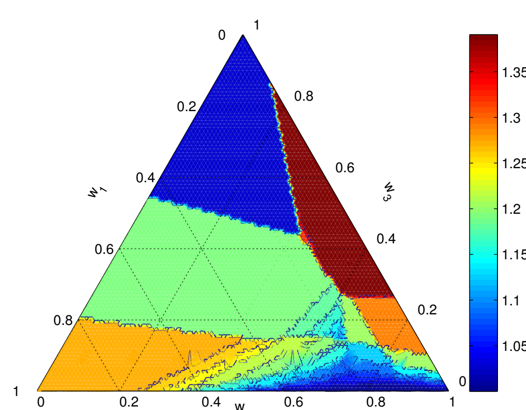

(f) ϵ

Fig. 9: Optimization results for $L = 3$ cm.

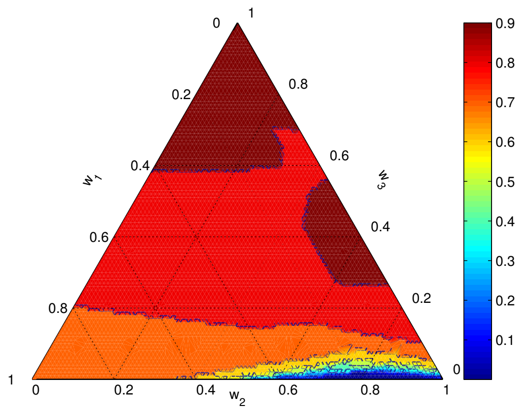

(**a**) optimum $\mathcal{C}$

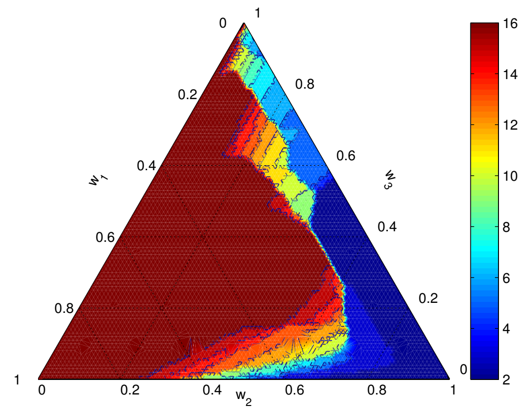

(**b**) optimum Q

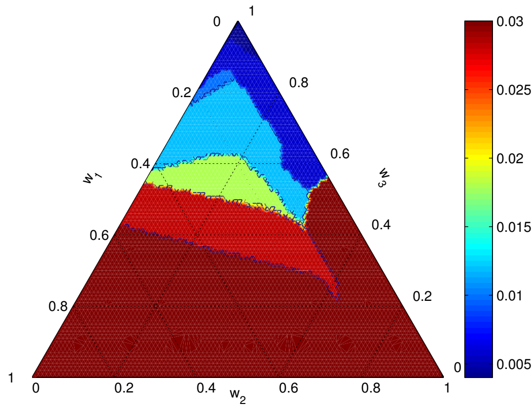

(**c**) optimum L

Fig. 10: Optimization results in the $\{\mathcal{C}, Q, L\}$ space.

general tool to make decisions on reactor configuration and operating conditions based on multiple, often mutually-conflicting criteria.

5 Acknowledgments

This work was funded by the French State through Banque Public d'Investissement in the framework of Fonds Unique Interministériel granted to BATIR project (AAP 14).

References

[1] T Belmonte, G Henrion, and T Gries. Nonequilibrium Atmospheric Plasma Deposition. *Journal of thermal spray technology*, 20(4):744–759, 2011.

[2] Hiroaki Kakiuchi, Hiromasa Ohmi, and Kiyoshi Yasutake. Atmospheric-pressure low-temperature plasma processes for thin film deposition. *Journal of Vacuum Science & Technology A*, 32(3):–, 2014.

[3] Volkmar Hopfe and David W Sheel. Atmospheric-pressure plasmas for wide-area thin-film deposition and etching. *Plasma Processes and Polymers*, 4(3):253–265, 2007.

[4] Daphne Pappas. Status and potential of atmospheric plasma processing of materials. *J. Vac. Sci. Technol. A*, 29(2):020801, 2011.

[5] Francoise Massines, Christian Sarra-Bournet, Fiorenza Fanelli, Nicolas Naudé, and Nicolas Gherardi. Atmospheric pressure low temperature direct plasma technology: Status and challenges for thin film deposition. *Plasma Processes and Polymers*, 9(11-12):1041–1073, 2012.

[6] Ionut Enache, Hubert Caquineau, Nicolas Gherardi, Thierry Paulmier, Louison Maechler, and Francoise Massines. Transport Phenomena in an Atmospheric-Pressure Townsend Discharge Fed by N2/N2O/HMDSO Mixtures. *Plasma Processes and Polymers*, 4(9):806–814, 2007.

[7] V. Hopfe, R. Spitzl, I. Dani, G. Maeder, L. Roch, D. Rogler, B. Leupolt, and B. Schoeneich. Remote microwave pecvd for continuous, wide-area coating under atmospheric pressure. *Chemical Vapor Deposition*, 11(11-12):497–509, 2005.

[8] Volkmar Hopfe and David W Sheel. Atmospheric-pressure PECVD coating and plasma chemical etching for continuous processing. *Plasma Science, IEEE Transactions on*, 35(2):204–214, 2007.

[9] J Benedikt, V Raballand, A Yanguas-Gil, K Focke, and A von Keudell. Thin film deposition by means of atmospheric pressure microplasma jet. *Plasma Physics and Controlled Fusion*, 49(12B):B419, 2007.

[10] I. Enache. *Etude expérimentale et modélisation du transfert de matière et des instabilités dans des décharges de Townsend à pression atmosphérique en mélange HMDSO-N_2O-N_2*. PhD thesis, Université Toulouse 3, 2007.

[11] B. Eliasson, W. Egli, and U. Kogelschatz. Modelling of dielectric barrier discharge chemistry. *Pure and Applied Chemistry*, 66(6), January 1994. time-scales.

[12] F. Massines, P. Ségur, N. Gherardi, C. Khamphan, and A. Ricard. Physics and chemistry in a glow dielectric barrier discharge at atmospheric pressure: diagnostics and modelling. *Surface and Coatings Technology*, 174–175:8–14, September 2003.

[13] Fiorenza Fanelli, Sara Lovascio, Riccardo d'Agostino, Farzaneh Arefi-Khonsari, and Francesco Fracassi. Ar/HMDSO/O2 Fed Atmospheric Pressure DBDs: Thin Film Deposition and GC-MS Investigation of By-Products. *Plasma Processes and Polymers*, 7(7):535–543, July 2010.

[14] Fiorenza Fanelli, Sara Lovascio, Riccardo d'Agostino, and Francesco Fracassi. Insights into the Atmospheric Pressure Plasma-Enhanced Chemical Vapor Deposition of Thin Films from Methyldisiloxane Precursors. *Plasma Processes and Polymers*, 9(11-12):1132–1143, December 2012.

[15] Igor Vinogradov and Achim Lunk. Film Deposition in the Dielectric Barrier Discharge at Atmospheric Pressure in He/O2/HMDSO and He/N2o/HMDSO mixtures. *Plasma Processes and Polymers*, 6(S1):S514–S518, June 2009.

[16] J Benedikt, D Ellerweg, S Schneider, K Rügner, Reuter R, H Kersten, and T Benter. Mass spectrometry of positive ions and neutral species in the effluent of an atmospheric pressure plasma with hexamethyldisiloxane and oxygen. *Journal of Physics D: Applied Physics*, 46(46):464017, 2013.

[17] J. L. Jauberteau and I. Jauberteau. Comparison of Hexamethyldisiloxane Dissociation Processes in Plasma. *The Journal of Physical Chemistry A*, 116(35):8840–8850, September 2012.

[18] R. Reuter, D. Ellerweg, A. von Keudell, and J. Benedikt. Surface reactions as carbon removal mechanism in deposition of silicon dioxide films at atmospheric pressure. *Applied Physics Letters*, 98(11):–, 2011.

[19] R. Reuter, N. Gherardi, and J. Benedikt. Effect of N2 dielectric barrier discharge treatment on the composition of very thin SiO2-like films deposited from hexamethyldisiloxane at atmospheric pressure. *Applied Physics Letters*, 101(19):194104, November 2012.